North-Gondwana -Laurussia dynamic paleogeography challenged by magnetic susceptibility through the Famennian

Girard Catherine, Feist Raimund, Mossoni Angelo, Jean-Jacques Cornee, Camps Pierre, Charruault Anne-Lise, Corradini Carlo, Catherine Girard, ; Feist, ; Mossoni, et al.

North-Gondwana - Laurussia dynamic paleogeography challenged by magnetic susceptibility through the Famennian

Girard, Catherine[1*]; Feist, Raimund[1]; Mossoni, Angelo[2]; Cornée, Jean-Jacques[3]; Camps, Pierre[3]; Charruault, Anne-Lise[1]; Corradini, Carlo[4]

[1]*Institut des Sciences de l'Evolution de Montpellier (ISEM), Univ Montpellier, CNRS, EPHE, IRD, Montpellier, France.*

[2] *2 Kingsdown court, 56 Bolingbroke grove, London SW11 6HS, UK*

[3] *Géosciences Montpellier, Université de Montpellier, CNRS, and Université des Antilles, Montpellier and Pointe à Pitre, (FWI), France*

[4] *Università degli Studi di Trieste, Dipartimento di Matematica e Geoscienze, Trieste, Italy*

*corresponding author (catherine.girard@umontpellier.fr)

Abstract

Large-scale magnetic susceptibility (MS) variations in ancient sediments are usually interpreted as related to sea-level and climate changes affecting the erosional regime and the amount of detrital input. To constrain such environmental changes during the Famennian, we compared MS records in representative sections of pelagic limestones of (1) the Avalonian margin of Laurussia [Sessacker (SES) and Beringhauser Tunnel (BHT), Rhenish Slate Mountains, Germany] and (2) in Gondwana related terranes [Erfoud (ERF), Tafilalt,

Morocco; Col des Tribes (CT), Montagne Noire, France; Buschteich (BU), Thuringia, Germany; Corona Mizziu (CM I, II), Sardinia and Pizzul West (PZW) in the Carnic Alps, Italy]. Very low MS values throughout the Famennian characterize sections from Avalonia. In contrast, MS values are high and oscillating in Gondwana during the early Famennian; they drop significantly all together in the middle Famennian *Palmatolepis marginifera marginifera* Zone to match the pattern of low MS values of the Avalonian margin thereafter. To evaluate the importance of partial diagenetic overprint, MS data were compared to hysteresis parameters and geochemical proxies in sections BU, CM I, II and CT. The degree of thermal diagenesis is estimates taking into account the Color Alteration Indices (CAI) of conodonts. Striking dissimilarities in MS records between Laurussia and Gondwana are in favor for an existing remnant oceanic barrier between these continents during early Famennian times, when the amount of detrital supplies was obviously different. Uniformity is reached after the drop of MS values in N-Gondwana, when oceanic barriers could have vanished during the early middle Famennian T-R fluctuations of the sea-level. All sites remained under a rather similar regime of detrital supply through middle to uppermost Famennian. Comparison of MS trends with trends of conodont biofacies in five sections (CT, BU, CM I, II and SES) allows emphasizing the concordance of their relationship to sea level fluctuations.

Keywords: magnetic susceptibility, conodont biofacies, Famennian, N-Gondwana, Laurussia, paleogeography

1. Introduction

Low-field magnetic susceptibility (MS) is currently considered a proxy to assess the amount of detrital inputs in relation to sea level changes, integrating mineralogical and sedimentological information on their nature and origin (e.g. Ellwood et al. 2006, 2007, 2008, Hladil 2002, Da Silva et al. 2009, 2010). As such it may constitute a powerful and independent proxy to control global trends of sea level changes on condition that the primary origin of low-field magnetic susceptibility is demonstrated. This can be done by comparing MS values with hysteresis parameters and/or elemental concentrations (Devleeschouver et al. 2010); Riquier et al. 2010). Color Alteration Indices (CAI) of conodonts are taken into account to estimate the degree of thermal diagenesis of the rock samples (Epstein et al. 1977). Indeed, the coulor of the conodonts is related to the temperature that affected the rocks. With an average MS value for lithified marine deposits of $5.5x10^{-8}$ m^3/kg (Ellwood et al. 2011a) most of Paleozoic limestones range between 0.1 and $10x10^{-8}$ m^3/kg (Ellwood et al. 2006). This is the case in Devonian off-shore carbonate successions where a fair number of MS investigations (e.g. Crick et al. 2002, Da Silva et al. 2009, Ellwood et al. 2011b, Riquier et al. 2010) were conducted since the first global sea-level curve was established by Johnson et al. (1985).

Comprehensive spatio-temporal investigations combining variations of litho- and biofacies with isotope data indicate a long term Famennian regressive trend (Johnson et al. 1985) that is punctuated by short transgressive episodes/events such as at the base of the Famennian (Sandberg et al. 2002). However, within-section MS evolution remains sometimes difficult to correlate with precision between sedimentary sequences from different paleogeographic entities (e.g., Crick et al. 2002). Attention is drawn to the possibility that MS signal in

[Tapez ici]

carbonate systems may be affected by diagenesis (Da Silva et al 2012, Devleeschouwer et al. 2015), or casually indicate rather particular local conditions (Davies et al. 2013) in spite of global eustasy.

Indeed, both the amount and nature of detrital material may possibly be disturbed by aeolian or volcanic inputs, heterogeneity of climatic influence in the continental source areas, and by the importance of physical action during gravitational transport (e.g., current-induced re-working, debris-massflows). On the contrary, slow sedimentation rates or absence of deposition leading to hardgrounds and hiatuses may result in different records of MS signals and their amplitudes. MS studies have been mainly focused on episodes of major extinction events such as the terminal Frasnian Kellwasser events that are particularly marked by instabilities of the sea-level (e.g., Averbuch et al. 2005, Riquier et al. 2010). According to these authors, the increase of detrital input related to the marked sea-level fall in the earliest Famennian post-event period is expressed by a significant increase in the MS signals. Noticeably, the values of this excursion is particularly less marked in sections on the Avalonian margin of Laurussia than in those of the Gondwana margin (Averbuch et al. 2005, fig. 4) (Fig. 1).

In this contribution we carry out investigations on the entire Famennian from representative sites of both N-Gondwanan and Avalonian terranes to allow the evaluation of the extent to which the environmental changes of approaching Laurussia/Gondwana margins may have influenced the MS signals (Fig. 1a). To this end, we conducted an integrated study of MS, hysteresis parameters and element concentrations, in some sections (CM I, CM II, PZW and partially in BU), in order to test whether MS can be considered as a reliable detrital proxy. Following Riquier et al. (2010), some elements characteristic of the terrigenous input are not affected by diagenesis (e.g., Zirconium) and can be used as a proxy of the bulk magnetic

mineralogical component (Total Fe). Thereafter, we will compare MS measurements with analyses of conodont biofacies in sections that provide sufficient amounts of conodont elements. Indeed, conodonts can also characterize palaeo-environments because of the different ecological preferences of the various genera (Sandberg 1976, Seddon and Sweet 1971, Girard et al. 2020), indicative of distance regarding the shoreline. According to this view, the changes in the relative proportion of the different genera, namely biofacies, have been proven useful to track environmental changes through time (e.g., Corradini 2003, Girard et al. 2014, 2017, 2020). As a prerequisite, the continuity of MS records is controlled by fine-scaled conodont biostratigraphy of Spalletta et al. (2017), updated in the latest Famennian by Corradini et al. (2021).

Whether trends in combined MS and biofacies curves allow constituting characteristic features of Famennian deposits in general, and to what extend they are permanent or are restricted to a definite duration, are prime subjects of our investigations. They allow pointing possible causes that we aim to discuss.

2. Famennian sections

The investigated sections, CT, BU, PZW, CM, ERF, BHT, SES (and DGHS for comparison) are situated between north Gondwana and Laurussia at tropical to subtropical paleolatitudes **(**Fig. 1a**)**. The position of some samples, conodont zones and main lithofacies are shown in columnar sections Figure 1b.

2.1. North Gondwana sections

Col des Tribes (Montagne Noire, France).

This section (72 m-thick) was described by Girard et al. (2014). It is composed of (from bottom to top): - bioclastic limestones (17 m- thick) organized into dm- thick beds; - massive, red mudstones to wackestones/floatstones (15 m- thick) organized into dm- thick beds yielding abundant cheiloceratid goniatites (Griottes facies); - massive micritic limestones (20 m- thick) organized into dm- thick beds; - pseudo-nodular limestones (15 m- thick) composed of cm- thick beds which have experienced pressure-dissolution processes; - massive micritic limestones (5 m- thick). These sediments were deposited in mid ramp to basin settings.

Abundance of conodonts allows establishing a fine–scaled biozonation from the *Pa. rhenana* (late Frasnian) to the *Bi. ultimus* Zone (*Pr. meischneri* Subzone, latest Famennian). In this section conodonts are relatively well preserved, with a low Conodont Alteration Index (CAI) ~ 2-2.5 (temperature range = 60 to 110°C).

Buschteich (Thuringia, Germany).

This section (35 m- thick) was studied by Girard et al. (2017). From bottom to top, it is composed of: - cm bedded to pseudonodular wackstones (3 m- thick) (Frasnian); - dm to m-thick beds of mudstones to wackestones (7 m- thick); - mud-wackestones and pseudonodular mudstones (7 m- thick); mm to cm- bedded mud-wackestones (10 m- thick); - mm to cm bedded to pseudonodular wackestones, and some clay (8 m- thick). These sediments were deposited in outer ramp to basin settings. The section spans an interval from the *Pa. rhenana* to *Bi. ultimus* (*Pr. meischneri* Subzone) conodont Zones, but the lowest part of the Famennian is missing (from *Pa. subperlobata* to *Pa. minuta minuta* Zones). The CAI of conodonts is high, estimated as 4 (temperature range = 190 to 300°C).

Pizzul West (Carnic Alps, Italia).

This section (24 m- thick) was described by Mossoni et al. (2014), and Corradini et al. (2017). From bottom to top, it comprises: - massive to nodular grey mudstones to packstones (16.5 m-thick); - red nodular wackestones to packstones (7.5 m- thick) (Griottes facies). The limestones contain few fossils. The Griottes facies comprises nodules up to 1 cm of diameter coated with hematite precipitations probably due to synsedimentary diagenesis. The sediments were deposited in mid to outer ramp settings. The section spans an interval from the *Pa. glabra prima* to *Pa. marg. marginifera* Zones. The CAI of conodonts is around (temperature range = 190 to 300°C).

Corona Mizziu I and Corona Mizziu II (Sardinia, Italia).

The Corona Mizzu sections have been studied by Corradini (1998, 2003).

The Corona Mizziu I (CM I) section (30 m- thick) comprises beds of poorly fossiliferous mudstones, with wackestone to packstone beds in the middle part of the succession. Sediments were deposited in a pelagic setting. The conodont data allow discriminating twelve conodonts zones from the *Pa. rhomboidea* Zone up to the *Bi. ultimus* Zone.

The Corona Mizziu II (CM II) section (18 m-thick) crops out a hundred meters apart from the CM I section and exposes grey massive monotonous mudstones with poor fossil remains. The tectonic imprint is marked by stylolite structures and calcite recrystallization. Sediments were deposited in a pelagic setting. The section spans a time from the *Pa. crepida* to the *Pa. rugosa trachytera* Zones. For these two sections (CM I and CM II), the CAI of conodonts is very high, with values near 4.5 – 5 (temperature range = 300 to 400°C).

Erfoud (Tafilalt, SE Morocco).

The Erfoud section spanning the entire Late Devonian has been described by Buggisch & Clausen (1972). The considered lower to middle Famennian part of the section (8 m- thick)

was re-sampled. It comprises from bottom to top: - 3 m-thick dark grey mud to wackestones and black shales, with dm-thick beds with cephalopods and bivalve remains (Kellwasser Limestone facies); - 0.45 m- thick platy red-brownish and grey-olive microsparitic calcilutites with bioclasts and Fe-oxid coated oncoids ; - 1.10 m-thick grey-brown cephalopod calcilutites with Fe-oxid coated intraclasts; - 1.95 m-thick thin-bedded nodular calcilutites with cephalopods and trilobites ; -1.50 m- thick alternating cm- thick bedded beige argillaceous nodular limestones and marls. In the lower part of the section the *Pa. crepida* Zone is extremely condensed at the top of the dysoxic black Kellwasser-type limestone. The latter characterises a dysoxic bottom sea depositional environment. Above the Kellwasser limestones, the depositonal conditions reflect low sedimentation rates in an open outer shelf environment within the photic zone as testified by prevaling large-eyed trilobites (deep inner to mid ramp). The section encompasses the interval of the *Pa. subperlobata* to the *Pa. rugosa trachytera* Zones with a gap between the *Pa. termini* to *Pa. gracilis gracilis* Zones (Fig. 1b). Conodonts have a CAI of 3-4 (temperature range = 150 to 300°C).

2.2. South Laurussia sections

Beringhauser Tunnel (Rhenish Slate Mountains).

This section (15 m- thick) was studied by Schülke & Popp (2005). It consists of mainly well-bedded massive to subordinately nodular cephalopod limestones. At the top of the section, facies change from massive limestones to nodular limestones. Sediments were deposited in mid to outer ramp setting. The considered section spans a time from the *Pa. crepida* to the *Pa. rugosa trachytera* Zones. The CAI of conodonts is high, about 4.5 (Joachimski et al. 2009), (temperature range around 300°C).

Sessacker (Rhenish Slate Mountains)

This highly condensed section (2.5 m- thick) was studied by Ziegler (1962) and Schülke (1999), and complemented by new data. It consists of red mudstones to wackestones with cephalopods, and some sparitic intercalations occur. The sediments were deposited in outer ramp setting. The section spans from the *Pa. delicatula platys* to the *Pa. rugosa trachytera* Zones. The conodonts are well-preserved with a CAI around 2.5 (temperature range = 60 to 110°C).

Dupont GHS drillhole (Illinois basin, Eastern North America).

Drillcores in the Chattanooga Shale of Illinois revealed fine-grained siliciclastic sediments (9 m- thick) dating Famennian (Over et al. 2019). Conodont assemblages indicate that the section spans the *Pa. glabra prima* to *Bi. ac. aculeatus* Zones. MS values are low, in the 0.25/-0.75 interval.

3. Methods

3.1. Magnetic Susceptibility

The samples studied are from previous collections for CT (Girard et al. 2014), BU (Girard et al. 2017), CMI and II (Mossoni 2014), PZW (Mossoni 2014). 129 new samples from sections SES, BHT and ERF have been analysed. We measured the low field magnetic susceptibility (χLF), abbreviates as magnetic susceptibility (MS) for the seven representatively distributed Famennian sections.

At Col des Tribes (CT, Montagne Noire, France) the field magnetic susceptibility (MS) was directly measured in situ with the Bartington MS2E sensor connected to the MS3 meter. To

ensure a representative result, five measures were performed and then averaged for the 74 successive stratigraphic levels (Supplementary Data, Table S1). Ex-situ measurements were performed in the laboratory on block samples from German (63 samples for BU, 26 for SES, and 15 BHT) and Moroccan (25 samples for ERF) sections with the same device and the same protocol involving a minimum of 2 measurements per level (Supplementary Data, Tables S2, S3, S4 and S5). Samples from the italian sections (Pizzul West and Corona Mizziu I, II were measured with the KLY-3S Kappabridge at the University of Liège (Supplementary Data, Tables S6, S7, S8).

All the MS data figured represent an average of the measurements (Fig. 2) expressed in 10^{-8} m^3/kg for readability. Following the age model published by Girard et al. (2020), the base of conodont zones was dated by means of absolute age estimates provided by Becker et al. (2012), and updated by Becker et al. (2020), and all MS data were figured based on the estimated absolute ages (Fig. 2).

3.2. Hysteresis parameters

The Italian sections (CM I, CM II and PZW) were prepared for hysteresis loops (Mossoni 2014) with the objective to roughly estimate the nature of the ferromagnetic (*sensu lato*) Fe oxides. Indeed, as red nodular facies occur in Pizzul West but not in Corona Mizziu sections, we have suspected significant differences in the nature, the oxidation state, and the concentration quantity of strongly oxidized Fe-oxides such as hematite in the former section, and non-oxidized Fe-oxides such as magnetite in the later section. The hysteresis loops were measured with the J-Coercivity "rotation" magnetometer at Dourbes IRM Geophysical Centre, respectively (Supplementary Data, Tables S8, S9, S10).

For the hysteresis measurements, the specimens were prepared from blocks taken every 10 cm all along the studied cross-sections. We calculated from the hysteresis loops the high-field magnetic susceptibility (χHF) and the ferromagnetic susceptibility (χferro) following methods developed in Riquier et al. (2010), and Da Silva et al. (2012, 2015). These two parameters allow assessing the respective contribution of the para/dia-magnetic minerals (χHF) and the ferromagnetic minerals to the initial susceptibility. At the end of the hysteresis loop acquisition, the magnetic viscosity coefficient was calculated from the remanence decay, which was monitored for 100s after the field was removed.

Additionally, the major elements (Al, Si, K and Ti) were considered to estimate the proportion of minerals in terms of their magnetic amounts for17 samples in PZW, 13 samples in CM I and 14 samples in CM II (Tables PZW, CM I and CMII). These analyses on major elements were performed with an X-Ray Fluorescence (Panalytical MagiX PW2540) device at the University of Cagliari. The powder disks were prepared using at least 20 grams of the sample mixed with polyvinyl alcohol, on a base of boric acid. The total amount of oxides and LOI (loss on ignition) has been considered acceptable for samples with an error of ±2%. In order to have comparable results between the studied sections, all analyses were normalized to 100. In this way a small error percentage has been distributed between all the measured parameters (Supplementary Data, Tables S8, S9, S10).

3.3. Detrital vs authigenic Fe content

To further constrain the diagenetic versus detrital imprints on MS, we compared the low-field magnetic susceptibility (χHF) variations with selected geochemical proxies measured by mean of the methods developed by Riquier et al. (2010). X-Ray Fluorescence analyses were performed on the samples of Buschteich which presents no signs of strong oxydation and is

the most complete section of this study. The analyses were performed with the Niton XL3900 Goldd X-ray fluorescence portable analyzer (Thermo Scientific®, Waltham, MA, USA) at the University of Montpellier. All the rock samples were carefully cleaned prior to all treatment, and weathered surfaces were removed.

We selected elements that can be used as proxies for the terrigenous input. The Zirconium (Zr) was selected here as the more reliable detrital proxy because it is not affected by diagenesis; and the total Fe (Fe_{tot}) content will be used as a proxy of the bulk magnetic mineralogical component. The total Fe was separated into an inherited detrital part and a secondary authigenic part. Following Riquier et al. (2010), the detrital and authigenic fractions of the total iron content were estimated considering that the Fe/Al ratio of the detrital part of the studied rocks is supposed to be the same as that of the average shale value ($Fe/Al_{average\ carbonate}$; 0.55 Clarkson et al. 2014). The detrital fraction of iron (Fe_{det}) is calculated as $Fe_{det} = Al_{sample} * Fe/Al_{average\ carbonate}$. Consequently, the iron fraction in excess relative to the detrital fraction, namely, $Fe_{exc} = Fe_{tot} - Fe_{det}$, may be considered to be of authigenic/diagenetic origin.

3.4. Biofacies

Five sections were sampled in detail for conodont biofacies based on conodont genera abundances. Conodont biofacies are advocated to be mostly driven by water depth variations due to the habitat preferences of the different conodont genera (e.g., Sandberg 1976, Seddon and Sweet 1971). In this regard, the distribution of conodont genera is thought to be controlled by water depth along a proximal-distal gradient (Klapper and Barrick 1978, Girard et al. 2020), and as such may constitute a proxy of sea-level variations and indirectly of detrital input. Several biofacies can be defined, based on the percentage of different genera present in the samples from biofacies characterized by distal surface dwellers (*Palmatolepis*)

to proximal surface dwellers (*Icriodus*). The percentages of conodont elements per genus, later on called biofacies, were estimated for samples of each section: 74 samples for CT (Girard et al. 2014), 34 samples for BU (Girard et al. 2017), 12 samples for SES (Schülke 1995; this study), 13 samples in CM I and 13 samples for CM II (Corradini 2003, Mossoni 2014). All data are available in the Supplementary Data, Table S11. As MS is also known to be related to detrital input, we compared the MS trends of these five sections with trends in percentage of conodont genera (biofacies). A Principal Component Analysis (PCA on the variance - covariance matrix) allows summarizing biofacies of the five considered sections (CT, BU, CM I and CM II, and SES) on few synthetic axes. This analysis also provides a representation of the records of CT, BU, CM I, CM II and SES on the same synthetic axes, allowing a direct comparison of the biofacies variations in the five outcrops. The contribution of each genus percentage to the axes allowed their interpretation in relation to the biofacies. Correlations between the MS and PC values are calculated using Pearson's product-moment correlation to investigate if MS and PC values are correlated or not.

4. Results

4.1. Magnetic susceptibility data

The relationship between the absolute age of the base of the biozone boundaries and sediment thickness allows establishing an age model for each section. The ages estimated for each sample were thereafter used to plot the variations of magnetic susceptibility through time. When we compare the evolution of magnetic susceptibility (MS) of Famennian sequences in the different sections, various types of record are documented (Fig. 2):

- In the investigated sections of the North Gondwana shelf (Morocco, Montagne Noire), MS values vary markedly and congruently during early Famennian times: initially high and

[Tapez ici]

fluctuating MS values shift all together to low ones within the *Pa. marginifera marginifera* Zone (initial mid-Famennian), and remain constantly low thereafter, lower than the common Paleozoic magnetic susceptibility values (around $5.5x10^{-8}$ m^3/kg).

- In the most distal sections of the Gondwana shelf (Sardinia, Carnic Alps, Thuringia), the same trend is observed but fluctuations are less pronounced during the lower Famennian with temporary increases in MS values before the *Pa. marginifera marginifera* Zone.

- In south Laurussia (DGHS section), the MS values remain low throughout the record, almost always less than the average of $5.5x10^{-8}$ m^3/kg, being rather close to the common Paleozoic magnetic susceptibility values.

- In the Avalonian outer shelf areas of Laurussia (SES and BHT), the MS values are very low during the early Famennian and are similar to those of both Laurentian (DGHS, Fig. 1) and north Gondwanan terranes during mid-through late Famennian times.

In summary, in the north Gondwana margin a two-fold stage subdivision of the magnetic susceptibility curve is observed. During the lower Famennian, increasing high values are first recorded then followed by decreasing values that culminate during the *Pa. marginifera marginifera* Zone. During the middle to upper Famennian, MS values remain lower than the common Paleozoic magnetic susceptibility values (vertical dotted line in Figure 2). The major shift from high to low MS values during the *Pa. marginifera marginifera* Zone in Gondwana is not recorded in the Laurussia section where MS values remain low through the entire Famennian.

4.2. Magnetic hysteresis data

For the Italian sections PZW, CM I and CM II, the correlations of oxides representing terrigenous input with the MS data are shown in the Supplementary Data (Fig. S1), and detailed in Table 1.

For the Pizzul West section, a significant correlation exists between the low field magnetic susceptibility (χ_{LF}) and ferromagnetic contribution (χ_{ferro}), but not with the high field magnetic susceptibility (χ_{HF}). A correlation between low field magnetic susceptibility (χ_{LF}) and the geochemical parameters is not observed (Al_2O_3=0.005, SiO_2=0.12, TiO_2=0.12, K_2O=0.04) (Table 1). However, there is a highly significant correlation between the high field magnetic susceptibility (χ_{HF}) and geochemistry (Al_2O_3=0.84, SiO_2=0.81, TiO_2=0.85, K_2O=0.83), that demonstrates that the paramagnetic fraction is linked to Al, Si, K and Ti bearing minerals.As most of the Hcr values are lower than 60mT, the MS variations are probably related to low coercivity minerals as magnetite.

For the CM I section a strong correlation exists between the low field magnetic susceptibility (χ_{LF}) and the high field magnetic susceptibility (χ_{HF}), and the ferromagnetic contribution (χ_{ferro}). This demonstrates that the paramagnetic fraction is linked to Al, Si, K and Ti bearing minerals. A very good correlation also exists between the low field magnetic susceptibilit and the four measured oxides (Al_2O_3=0.68, TiO_2=0.70, K_2O=0.69) (Table 1).

For the Corona Mizziu section II, the low field magnetic susceptibility has a good correlation with χ_{ferro} (r = 0.85) and with χ_{HF} (r = 0.82) (Table1). This suggests that the low field magnetic susceptibility of the Corona Mizziu II section is controlled by both the ferromagnetic and paramagnetic contributions. All the MS values are extremely low (lower than 3.0×10^{-8} m^3/kg, indicating the influence of the diamagnetic fraction, which may have diluted the potential detrital signal.

The magnetic signal for Pizzul West section would be mainly controlled by ferromagnetic contribution of low coercivity mineral (likely magnetite), whereas, for the Corona Mizziu I and II sections, the magnetic signal seems to be influenced by dia and/or paramagneticcontributions and, to a lesser extent, by ferromagnetic contribution.

363 *4.3. MS correlation to Fe content*

364 Both measured Fe_{tot} and calculated Fe_{det} correlate with the MS evolution (r = 0.46, p = 0.002
365 for Fe_{det} and r = 0.41; p = 0.0005 for total Fe). The Fe_{exc} does not show a correlation with the
366 MS variations (r = 0.19, p = 0,157). A correlation exists between MS and the Zr content 367
(r=0.28, p = 0.037) as well as between the MS and the Fe/Zr ratio (r=0.73, p<0,001).

368 (Supplementary Data, Fig. S2 and Supplementary Data, Table S2). Although this theoretical
369 calculation gives an estimate of the Fe-bearing fractions only, Fe_{det} and Fe_{exc}, it supports the
370 coexistence of a detrital component, controlling the MS evolution in Buschteich, and an
371 authigenic component, that could have induced the widespread remagnetization process
372 observed in these carbonates. This means that for the Buschteich section we cannot exclude
that a part of the signal results from diagenetic processes, but this part is not as significant as
374 the detrital part.
375 In summary, the geochemical data show that, although in part affected by diagenesis, as
376 shown by correlation between MS and Fe/Zr, MS can be used as an indicator of the detrital
377 input evolution in the studied Famennian sections. It is consequently possible to use it as a
proxy of sea level variations which can be compared to the conodont biofacies proxy.
379

380 *4.4. Comparison with conodont biofacies*

381 The principal component analysis performed on the proportions of different genera allows
382 summarizing the biofacies variations (Fig. 3) on main axes that express the total variance. The
383 record of the five sections CT, BU, CM I, CM II (North Gondwana) and SES (South
Laurussia) can be directly compared on these axes.

385 The first axis (PC1, 75.8% of the total variance) of the principal component analysis on

conodont percentages shows a progressive trend to positive values (from 0 to 1) through the early Famennian. This trend reverses in the early mid – Famennian to negative values (Fig. 3b). The contribution of the variables (here, the percentages of the different genera) to the axes (Fig. 3b) shows that positive values along the first axis correspond to a high proportion of *Palmatolepis* whereas negative values correspond to a high proportion of *Bispathodus* (Supplementary Data, Table S11). A correlation ($N = 115$; $r = 0.26$; $p < 0.005$) exists between the PC1 and the MS data. The third axis represents only < 4% of variance, and mostly corresponds to variations in the proportion of *Icriodus* in the early Famennian : peaks from *Pa. triangularis* to *Pa. crepida* Zones in CT, peak in the *Pa. crepida* Zone in BU, peak from the *Pa. glabra prima* to the *Pa. rhomboidea* Zones for CM, peak from *Pa. delicatula platys* to *Pa. minuta minuta* in SES (Supplementary Data, Table S1, and Fig. 3c), but values on the PC3 axis are not correlated with the MS values.

5. Discussion

Since pelagic carbonates are dominantly microsparites of diagenetic origin (Franke & Walliser 1983), one can only speculate on the ultimate source of the MS signals as these may be variously impacted by post-depositional processes. Following intervening aspects are discussed:

5.1. Impact of diagenesis

The magnetic susceptibility of a rock depends on both the mineralogical composition of the rock and the proportion of each mineral. The three main magnetic behaviours are: diamagnetic minerals (such as carbonates and quartz) displaying extremely weak negative MS values; paramagnetic minerals (e.g., clay minerals, particularly chlorite, smectite, illite and

glauconite, ferromagnesian silicates, iron and manganese carbonates, pyrite) displaying weak positive values, and ferromagnetic minerals (mainly magnetite, pyrrhotite, maghemite, and hematite) displaying strong positive values (Da Silva et al. 2010). Diagenetic and post diagenetic processes lead to mineralogical and chemical transformation of iron oxides that in turn influences the MS values. Riquier et al (2010) showed that although submitted to different burial histories and diagenetic conditions, consistent long-term trends can be observed in the MS evolution from sections through the Frasnian-Famennian boundary. Their data demonstrated that the MS evolution of the carbonate sections they studied can be interpreted in terms of paleoenvironmental changes along the former margins of Laurussia and Gondwana.

In Pizzul West and Corona Mizziu, the conodont Color Alteration Index (CAI) ranges between 4.5 – 5.5. The temperature (200-400°C) which affected the rocks is far beyond the temperature of the goethite-hematite transition. Thus, the high coercivity values measured are related to the presence of hematite, visible also in the microfacies (Mossoni 2014). However, where high coercivity minerals control the MS (χLF), the presence of hematite is here interpreted to be of detrital origin because both the high field magnetic susceptibility (χHF) and the viscous decay do not correlate.

At Buschteich, the Fe in excess does not modify the general trend of MS, at least not enough to overprint the detrital signal.

In the CT section, CAI values of 2 – 2.5 were measured by Wiederer et al (2002), that corresponds to burial temperature of less than 100°C. Low illite crystallinity indicates that the site underwent anchizonal metamorphism at maximum. We assume therefore that a part of the MS signal, associated to iron-bearing primary clay minerals, has been preserved in the NGondwana sections despite different diagenetic stories.

Trends in MS are similar on the N-Gondwana margin (CAI estimed to 4-5 in PZW, CMI and II, BU and around 2-2.5 for CT), high values during the early Famennian and low values during mid-late Famennian. Similar patterns also occur in the S-Laurussia margin (CAI near 4 for BHT and only 2-2.5 for SES), but values remain low during the Famennian. This indicates that, despite different burial histories, the primary MS signature was not overprinted by the diagenetic signal, and it reflects in part its detrital origin.

5.2. Relations between depositional setting and MS

Variations in the amount of detrital ferromagnetic minerals in off-shore cephalopod limestones may be of different origins, and, in consequence, it is often difficult to precisely determine the cause of changing MS values and their amplitudes (e.g. Devleeschouver et al. 2015). In this regard, the depositional conditions of the investigated sections could play a role on the accumulation of ferromagnetic minerals.

In the Rhenish Slate Mountains (SES, BHT), the Upper Devonian cephalopod limestones were deposited upon deep submarine rises beyond direct influence of sea-level changes (Franke & Walliser 1983). Besides *in situ* precipitation, pelagic carbonate mud originated from shallow-water areas. Fine-grained sand and clay fractions, originated from distal turbidites deposition, have also probably reached the rises but they mostly have been winnowed away by bottom currents. Consequently, rather low MS values might reflect presence low amount of transported ferro-magnetic elements, as coarse detrital influxes from northern shelf margins were concentrated in sandstone turbidite bodies that by-passed and were dispatched in troughs between the rises.

In the Montagne Noire (CT), very high MS values are recorded during the *Pa. marginifera marginifera* Zone prior to a sudden shift to low values under more stable environmental

conditions in deeper mid-Famennian outer ramp setting. This shift is coincident with an abrupt change in facies: high though strongly oscillating values are found in the famous red-colored Griottes facies (Tucker 1974) and low values in the overlying compact light grey carbonate mudstones. The Griottes facies is a cephalopod-rich, nodular limestone with abundant iron-clay coatings and some ferruginous hard-grounds. The MS values in this facies are influenced by different chemical and/or physical constraints, not only the detrital inputs of ferro-magnetic minerals. Indeed, ferrugineous mineral phases accumulations may also be influenced by changing both bottom sea oxygenation and rates of Fe-oxide –reduction related to buried organic matter and to diagenetic re-precipitation of Fe-oxide (Franke & Paul 1980). This is the case, for example, of condensed pelagic carbonates across the Givetian/Frasnian boundary, where Devleeschouwer et al. (2015) drew attention to the fact that the ferro-magnetic fraction may contain high coercivity minerals such as hematite and goethite of secondary origin that could affect the MS signal. This is probably also the case in the CT section, but no hysteresis analyses are available to confirm the assumption that the observed positive excursions may be solely related to hematization during diagenesis. Post-depositional transformation of paramagnetic clay minerals may also alter the detrital signal of MS. However, this is not the case because the burial temperature was less than 100° (CAI 2-2.5) in CT (Wiederer et al. 2002). It is noteworthy however, that, at CT, the Griotte limestones were deposited on an unstable slope under current activity and underwent repeated intra-formational submarine sliding (debris flows, slumping…) (Girard et al. 2014), leading to local accumulation of Fe-rich sediments. These events may correspond to anomalously high positive peaks in the MS curve at the base of the *Pa. marginifera marginifera* Zone (Fig. 2). At the basins scale, the scenario of MS positive excursions coinciding with hematite-rich early Famennian Griotte limestones has to be discussed. The Griottes limestones are

commonly found in southern Europe including the Pyrenees, Montagne Noire and Carnic Alps. Nevertheless, they do not exist in contemporaneous strata in Sardinia despite a similar MS signal. Moreover, this facies is not present in the Thuringian Buschteich section where the MS variation pattern is the same. Conversely, at the beginning of the mid-Famennian, high MS values characterize also compact reddish and brown calcilutites with iron-oxide coatings on the shallow northern Tafilalt platform subjected to emergences (Buggisch & Clausen 1972, Wendt & Aigner 1985). It is noteworthy that a different scenario prevails in the Rhenish slate-mountains where condensed carbonate deposits on deep-water submarine rises upon volcanic substrates at Sessacker are red-coloured despite rather low MS values. At BHT similar low values, after a marked positive excursion in the earliest Famennian (Riquier et al. 2010), occur in mud-mound carbonates which are not red-colored (Schülke & Popp 2005).

In summary, the MS variations during the Famennian is independant from the presence of red facies (Griottes or others), and are consequently interpreted as primary. Consequently, the effect of post-depositional processes probably did not significantly overprint those of sea level changes during the Famennian to explain the differences between the records of Gondwana and Laurussia, especially the high MS values during the early Famennian in North Gondwana.

5.3. Influence of sea-level changes

Magnetic susceptibility and conodont biofacies are potentially interrelated: MS could be a proxy to evaluate detrital input if the signal is of primary origin, and conodont biofacies are interpreted as related to water depth due to habitat preferences of the different conodont genera along a proximal-distal gradient in the surface waters. Conodont PC1 displays a strong relationship with magnetic susceptibility in N-Gondwana terranes, and also on Laurussia, at

[Tapez ici]

506 least for Sessacker, and as such suggests constituting a real indicator of sea-level variations
507 during the Famennian: low MS signals indicate a transgressive trend and correspond to distal biofacies, and, inversely, high MS signals indicate a regressive trend and correspond to proximal biofacies.

510 The shift towards lower values for MS and the trend to negative values on the PC1 in
511 N-Gondwana terranes coincides with a local T-R (transgressive - regressive) couplet called
512 "Enkeberg event" described in Laurussia (Rhenish Slate Mountains; House 1985). In
513 Avalonia (Laurussia), there is no major significant change in MS values but the Enkeberg
514 event was identified in the faunal record (Becker 1993). This event has not been yet identified in the North Gondwana terranes. Consequently, the differences in the MS records of Gondwana and S-Laurussia rely on other factors, such as paleoclimate and paleogeography.

517

518 *5.4. Paleoclimate and paleo-latitude*

535 During the Famennian, SES, BHT, BU, and PZW sections were located in the subtropical zone of the southern hemisphere (Fig. 1). A long-term discrete cooling occurred during the Famennian, but no major changes in temperatures of the sea-surface waters was recorded (Joachimski et al. 2009); this may exclude a major role of physico-chemistry parameters of sea water conditions on MS values. Following the draw-down of atmospheric CO2 concentrations and burial of organic carbon during the end-Frasnian Kellwasser crises, oxygen isotope values in conodont apatite indicate a global mean temperature drop of low latitude surface-water in post-event early Famennian times (Balter et al. 2008; Joachimski & Buggisch 2002; Joachimski et al. 2009). Mean sea-surface temperatures estimated from conodont apatite δ18O values in the Rhenish Slate Mountains (Beringhauser Tunnel section) seem to be slightly higher than in Gondwana related terranes (Thuringia, Carnic Alps, Southern France) (Joachimski et al. 2009). Concerning climate, the main difference between

536 Gondwana and Laurussia could rely on the latitudinal position between sites on the subtropical Laurussia and those of North Gondwana that are farther south in a more temperate

position. Indeed, emerged parts of North Gondwana would have accentuated seasonality of climate and enhanced continental weathering (Percival et al. 2019; Herman et al. 2013).

Therefore, emerged areas within the North Gondwana domain might have provided larger amounts of detrital material than the emerged parts of Laurussia. The decrease of high MS values on the Gondwana shelf began during the *Pa. rhomboidea* highstand of sea level and was probably achieved during the following transgressive pulse of the Enkeberg Event during the early mid-Famennian (Sandberg et al. 2002).

5.5. Dynamic paleogeography

Though still debated, Late Devonian plate tectonic models postulate convergence and collisional events between Gondwana and Laurussia heralding both the onset and the development of the Variscan orogeny. Subduction of oceanic crusts between Gondwana-derived continentsled successively to the closure from S to N of several oceanic basins (including, Saxo-Thuringian, Rheno-Hercynian oceans...) that previously separated Armorican terranes (e.g., Thuringia, Bohemia) from the southern Laurussian margin (Franke et al. 2017, Golonka 2020) (Fig. 1). This resulted in the formation of large carbonate platforms on distal marine shelves on the Gondwana margins (parts of NW Africa to Montagne Noire). Opposite, on the southern margin Laurussia (Thuringia microcontinent), condensed pelagic limestones were restricted to tectonic or volcanic submarine highs.

During the early Famennian, only the narrowing oceanic interspaces of the Rheno-hercynian basin, assumed width was 1000 km during the Frasnian, separated Laurussia from outer-shelves of Gondwana-derived terranes (Franke et al. 2017). The age of the closure of the Rheic Ocean remains debated. After Franke (2019) it closed during the Early Devonian times. Other models maintained the Rheic

ocean open between Saxo-Thuringia and Avalonia until the Carboniferous (Eckelmann et al. 2014; Golonka 2020, fig. 4).

Nevertheless, all these models consider that the northern Gondwana shelf was much more extensive during the Famennian than those of South Laurussia which were restricted to narrow submarine highs and troughs. In such a setting, the detrital supplies from emerged source areas to carbonate platforms were naturally more homogenously dispatched in the N-Gondwana shelf than in the Laurussia margin. Opposite, the accumulation of the detrital material in the Laurussia margin, even if locally important, was in fact located in troughs (e.g., Rhenish area) and low MS values are recorded on the rises. Consequently, the N-Gondwana and South Laurussia margins clearly underwent a different paleogeographic behavior, and thus a different setting for detrital accumulation.

The separation between the two margins by the narrowing Rheno-Hercynian Ocean is effective at least until the beginning of the mid-Famennian, even if some local pelagic deposits can be found till the early Carboniferous (Franke et al. 2017). From the *Pa. marginifera marginifera* Zone onwards to the latest Famennian the effectiveness of the separation apparently vanished when climate became cooler (Girard et al. 2020). MS values considerably dropped and became conform to median values throughout the entire region between the Avalonian margins of Laurussia and N-Gondwana related terranes. Consequently, more uniform conditions and smaller amounts of detrital supply prevailed throughout. Concomitantly, the conjunction of vicinity of the two margins and similar climatic conditions is also corroborated by the increasing identity of stenotopic level-bottom biotas such as phacopid trilobites (Feist 2019) in both areas. Consequently, during this time interval, we condider that mid-late Famennian deposits with low MS values seems to be controlled by first an evolving paleogeographic setting, and, at a lesser extent, eustasy, current

activity and climate. This paleogeographic setting results from converging margins prior to closure, and questions the existence, during mid-late Famennian, of wide oceanic domains.

Conclusions

The MS study of five sections in the N-Gondwana margin shows high and oscillating values during the early Famennian, and low values during the mid-late Famennian. In the S-Laurussia margin, MS values remain low through the whole Famennian. Geochemical investigations, and hysteresis parameters in three N-Gondwana sections indicate that the diagenetic processes did not significantly overprint the primary signal of MS. This is emphasized by the degree of burial, thus the temperature during diagenesis (CAI of conodonts) and the presence or absence of red facies, as the MS values remain consistent from one section to other.

For the first time, we demonstrate a high correlation between these MS and conodont biofacies, confirming their validity for sea level reconstructions. Taking into account all the above mentioned studies, MS can now be used for paleogeographic reconstructions in the presently dismembered areas of the Variscan Belt.

During the early Famennian, the difference in the MS trends and the high values in N-Gondwana compared to S-Laurussia can be explained by two main paleogeographic constraints: i) the Rheic Ocean was not closed; ii) the North-Gondwana margin was wide whilst the South Laurussia margin was fragmented into rises and troughs. During the mid-late Famennian, the uniformization of MS toward low values is interpreted as indicative of rather similar conditions in both margins, linked to plate convergence and vanishing influence of oceanic spaces.

Declaration of competing interest

The authors declare that they have no known competing financial interests or personal relationships that could have appeared to influence the work reported in this paper.

Acknowledgements

This contribution profited substantially from critical remarks and constructive suggestions provided by W. Franke and an anonymous reviewer for which we are most grateful. We acknowledge the assistance of Thomas Tirard, Lucas Tortarolo, and Lisa Zaharias for measurements of Buschteich and Col des Tribes during their third-year university degree. Authors thank Eberhart Schindler who provided samples from Sessacker, and Bernard Orth for his assistance during the field-work in Morocco. A.M. thanks Anne Christine Da Silva and Dr Simo Spassov for their help with the issues of the magnetic susceptibility and for allowing him to work in their laboratories. This research was funded by the ANR project ECODEV (ANR-13-BSV7-005). This is contribution ISEM 2021-111.

References

Averbuch, O., Tribovillard, N., Devleeschouwer, X., Riquier, L., Mistiaen, B., Van Vliet Lanoe, B., 2005. Mountain building-enhanced continental weathering and organic carbon burial as major causes for climatic cooling at the Frasnian-Famennian boundary (c. 376 Ma)? Terra Nova 17, 25-34.

Balter, V., Renaud, S., Girard, C., Joachimski, M.M., 2008. Record of climate-driven morphological changes in 376 Ma Devonian fossils. Geology 36, 907-910.

Becker, R.T., 1993. Anoxia, eustatic changes, and upper Devonian to lowermost Carboniferous global ammonoid diversity, In: House, M.R. (Ed.), The Ammonoidea: Environment, Ecology, and Evolutionary Change. Systematics Assoc. Spec. Vol., Oxford, pp. 115-163.

Becker, R.T., Gradstein, F.M., Hammer, O., 2012. The Devonian Period, in: Gradstein, F.M., Ogg, J.G., Schmitz, M.D., Ogg, G.M. (Eds.), The Geologic Time Scale 2012. Elsevier, Oxford, pp. 559-602.

Becker, R.T., Marshall, J.E.A., Da Silva, A.-C., 2020. The Devonian Period. In Geological Time Scale 2020. doi: https://doi.org/10.1016/B978-0-12-824360-2.00022-X

638 Buggisch, W., Clausen, C.-D., 1972. Conodonten- und Goniatiten-Faunen aus dem oberen 639 Frasnium und unteren Famennium Marokkos (Tafilalt, Antiatlas). Neues Jahrb. Geol. 640 Palaontol. Abh. 141, 137-167.

641 Clarkson, M.O., Poulton, S.W., Guilbaud, R., Wood, R.A., 2014. Assessing the utility of
642 Fe/Al and Fe-speciation to record water column redox conditions in carbonate-
rich 643 sediments. Chem. Geol. 382, 111-122.

644 Corradini, C., 1998. Famennian conodonts from two sections near Villasalto. Giorn. Geol. 60,
645 Spec. Issue, 122-135.

646 Corradini, C., 2003. Late Devonian (Famennian) conodonts from the Corona Mizziu Sections
647 near Villasalto (Sardinia, Italy). Palaeontogr. Ital. 89, 65-116.

648 Corradini C., Mossoni A., Corriga M.G., Spalletta C., 2021. The Devonian/Carboniferous
649 Boundary in Sardinia (Italy). Paleobiodivers. Paleoenviron. 101. doi: 10.1007/s12549-
650 019-00411-5

651 Corradini, C., Mossoni, A., Pondrelli, M., Simonetto, L., 2017. Famennian conodonts in the
652 Mt. Pizzul West (PZW) section. Ber. Inst. Erdwiss. K.F.-Univ. Graz, 23, 246-250.

653 Crick, R.E., Ellwood, B.B., Feist, R., El Hassani, A., Schindler, E. Dreesen, R. Over, D.J., 654 Girard, C., 2002. Magnetostratigraphy susceptibility of the Frasnian/Famennian boundary.
655 Palaeogeogr. Palaeoclimatol. Palaeoecol. 181, 67-90.

656 Da Silva A.C., Mabille C., Boulvain F., 2009. Influence of sedimentary setting on the use of
657 magnetic susceptibility: examples from the Devonian of Belgium. Sedimentology 56,
658 1292-1306.

659 Da Silva A.C., Yans J., Boulvain F., 2010. Sedimentology and magnetic susceptibility during
660 the "punctata" event of the Ardenne area (Belgium): identification of severe and rapid sea 661 level fluctuations. In: Da Silva, AC. and Boulvain, F. (eds): magnetic susceptibility, 662 correlations and Palaeozoic environments. Geol. Belg. 13/4, 319-332.

663 Da Silva, A.-C., Whalen, M.T., Hladil, J., Chadimova, L., Chen, D., Spassov, S., Boulvain,
664 F., Devleeschouwer, X., 2015. Magnetic susceptibility application: a window onto ancient 665 environments and climatic variations: foreword. Geol. Soc. Spec. Publ., London 414, 1-
666 13.

667 Da Silva, A.C., Dekkers, M.J., Mabille, C., Boulvain, F., 2012. Magnetic signal and its 668 relationship with paleoenvironments and diagenesis - examples from the Devonian 669 carbonates of Belgium. Studia Geophys. Geod. 56, 677-704.

670 Davies, E.J., Ratcliffe, K.T., Montgomery, P., Pomar, L., Ellwood, B.B., Wray, D.S., 2013.
671 Magnetic Susceptibility (χ) Stratigraphy and Chemostratigraphy Applied to an Isolated
672 Carbonate Platform Reef Complex; Llucmajor Platform, Mallorca, In: Verwer, K.,
673 Playton, T.E., Harris, P.M.M. (Eds.), Deposits, Architecture, and Controls

674 Devleeschouwer, X., Petitclerc, E., Spassov, S., Préat, A., 2010. The Givetian-Frasnian 675 boundary at Nismes parastratotype (Belgium): the magnetic susceptibility signal controlled
676 by ferromagnetic minerals. Geol. Belg., 14/4, 345-360.

677 Devleeschouwer, X., Riquier, L., Bábek, O., Devleeschouwer, D., Petitclerc, E., Sterckx, S.,
678 Spassov, S., 2015. Magnetization carriers of gry to red deep-water limestones in the GSSP
679 of the Givetian-Frasnien boundary (Puech de la Suque, France): signals influenced by
680 moderate diagenetic overprinting, In: Da Silva, A.C., Whalen, M.T., Hladil, J.,

681 Chadimova, L., Chen, D., Spassov, S., Boulvain, F., Devleeschouwer, X. (Eds.), Magnetic 682 Susceptibility Applications: A Window onto Ancient Environments and Climatic 683 Variations. Geol. Soc. Spec. Publ., London 414 (1), 157-180.

684 Eckelmann, K., Nesbor, H.-D., Königshof, P., Linnemann, U., Hofmann, M., Lange, J.-M.,
685 Sagawe, A., 2014. Plate interactions of Laurussia and Gondwana during the formation of
686 Pangaea — Constraints from U–Pb LA–SF–ICP–MS detrital zircon ages of Devonian and 687 Early Carboniferous siliciclastics of the Rhenohercynian zone, Central European 688 Variscides. Gondwana Res. 25, 1484-1500.

689 Ellwood B.B., Garcia-Alcalde J.L., El Hassani A., Hladil J., Soto, F.M., Truyols-Massoni, M.,
690 Weddige, K., Koptikova, L., 2006. Stratigraphy of the Middle Devonian Boundary:
Formal 691 Definition of the Susceptibility Magnetostratotype in Germany with
comparisons to 692 Sections in the Czech Republic, Morocco and Spain. Tectonophysics
418, 31-49.

693 Ellwood B.B., Tomkin J., Richards B., Benoist S.L., Lambert L.L., 2007. MSEC Data Sets
694 Record Glacially Driven Cyclicity: Examples from the Arrow Canyon Mississippian695
Pennsylvanian GSSP and Associated Sections. Palaeogeogr. Palaeoclimatol. Palaeoecol. 696
255, 377-390. doi: 10.1016/j.palaeo.2007.08.006.

697 Ellwood B.B., Tomkin J.H., Ratcliffe K.T., Wright M., Kafafy A.M., 2008. High-resolution
698 magnetic susceptibility and geochemistry for the Cenomanian/Turonian boundary GSSP 699
with correlation to time equivalent core. Palaeogeogr. Palaeoclimatol. Palaeoecol. 261,
700 105-126.

701 Ellwood, B.B., Algeo, T., El Hassani, A., Tomkin, J.H., Rowe, H., 2011a. Defining the 702
Timing and Duration of the Kačák Interval within the Eifelian/Givetian Boundary GSSP,
703 Mech Irdane, Morocco, Using Geochemical and Magnetic Susceptibility Patterns.
704 Palaeogeogr. Palaeoclimatol. Palaeoecol. 304, 74–84.

705 Ellwood, B.B., Balsam, W.L., Roberts, H.H., 2006. Gulf of Mexico Sediment Sources and
706 Sediment Transport Trends from Magnetic Susceptibility Measurements of
Surface 707 Samples. Mar. Geol. 230, 237–248.

708 Ellwood, B.B., Tomkin, J.H., El Hassani, A., Bultynck, P., Brett, C.E., Schindler, E., Feist,
709 R., Bartholomew, A.J., 2011b. A climate-driven model and development of a floating point
710 time scale for the entire Middle Devonian Givetian Stage: A test using
711 magnetostratigraphy susceptibility as a climate proxy. Palaeogeogr. Palaeoclimatol. 712
Palaeoecol. 304, 85-95.

713 Epstein, A., Epstein, J., Harris, L. 1977. Conodont Color Alteration - an Index to Organic 714
Metamorphism. Geol. Surv. Prof. Pap. 995, 1-27. doi:10.3133/pp995.

715 Feist, R., 2019. Post-Kellwasser event recovery and diversification of phacopid trilobites in 716
the early Famennian (Late Devonian). Bull. Geosci. 94, 1-22.

717 Franke, W. Walliser, O.H. 1983. “Pelagic” carbonates in the Variscan Belt – their 718
sedimentary and tectonic environments, In: Martin H. and Eder F. W., Intercontinental
719 Fold Belts. Springer, Berlin, pp. 77-92.

720 Franke, W., Cocks, L.R.M., Torsvik, T.H., 2017. The Palaeozoic Variscan oceans revisited.
721 Gondwana Res. 48, 257-284.

722 Franke, W., Cocks, L.R.M., Torsvik, T.H., 2019. Detrital zircons and the interpretation of
723 palaeogeography, with the Variscan Orogeny as an example. Geol. Mag. 157 (4), 1-
5. 724 doi.org/10.1017/S0016756819000943

725 Franke, W., Paul, J. 1980. Pelagic redbeds in the Devonian of Germany – deposition and 726
diagenesis. Sediment. Geol. 25, 231-256.

727 Girard, C., Cornée, J.-J., Charruault, A.-L., Corradini, C., Weyer, D., Bartzsch, K.,
728 Joachimski, M.M., Feist, R., 2017. Conodont biostratigraphy and palaeoenvironmental 729
trends during the Famennian (Late Devonian) in the Thuringian Buschteich section 730
(Germany). Newsl. Stratigr. 50, 71-89.

731 Girard, C., Cornée, J.-J., Corradini, C., Fravalo, A., Feist, R., 2014. Palaeoenvironmental 732
changes at Col des Tribes (Montagne Noire, France), a reference section for the Famennian
733 of north Gondwana-related areas. Geol. Mag. 151, 864-884.

734 Girard, C., Cornée, J.-J., Joachimski, M.M., Charruault, A.-L., Dufour, A.-B., Renaud, S., 735
2020. Paleogeographic differences in temperature, water depth and conodont biofacies 736
during the Late Devonian. Palaeogeogr. Palaeoclimatol. Palaeoecol. 549, 108852.
737 https://doi.org/10.1016/j.palaeo.2018.06.046

738 Golonka, J., 2020. Late Devonian paleogeography in the framework of global tectonics.
739 Global Planet. Change 186. https://doi.org/10.1016/j.gloplacha.2020.103129

740 Herman, F., Seward, D., Valla, P.G., Carter, A., Kohn, B., Willett, S.D., Ehlers, T.A., 2013.
741 Worldwide acceleration of mountain erosion under a cooling climate. Nature 504.

742 Hladil, J., 2002. Geophysical records of dispersed weathering products on the Frasnian
743 carbonate platform and early Famennian ramps in Moravia, Czech Republic: proxies for 744
eustasy and palaeoclimate. Palaeogeogr. Palaeoclimatol. Palaeoecol. 181, 213-250.

745 House, M.R., 1985. Correlation of mid-Palaeozoic ammonoid evolutionary events with global
746 sedimentary perturbations. Nature 313, 17-22.

747 Joachimski, M., Buggisch, W., 2002. Conodont apatite $\delta^{18}O$ signatures indicate climatic 748
cooling as a trigger of the Late Devonian mass extinction. Geology 30, 711-714.

749 Joachimski, M.M., Breisig, S., Buggisch, W., Talent, J.A., Mawson, R., Gereke, M., Morrow,
750 J.R., Day, J., Weddige, K., 2009. Devonian climate and reef evolution: Insights from
751 oxygen isotopes in apatite. Earth Planet. Sci. Lett. 284, 599-609.

752 Johnson, J.G., Klapper, G., Elrick, M., 1996. Devonian transgressive-regressive cycles and 753
biostratigraphy, Northern Antelope Range, Nevada: establishment of reference horizons 754
for global cycles. Palaios 11, 3-14.

755 Johnson, J.G., Klapper, G., Sandberg, C.A., 1985. Devonian tatic fluctuations in Euramerica.
756 Geol. Soc. Am. Bull. 96, 567-587.

757 Klapper, G., Barrick, J.E., 1978. Conodont ecology: pelagic versus benthic. Lethaia 11, 15-
758 23.

759 Mossoni, A., 2014. Selected Famennian (Late Devonian) events (Condroz, Annulata,
760 Hangenberg) in Sardinia and in the Carnic Alps: conodont biostratigraphy, magnetic
761 susceptibility and geochemistry, Università degli Studi di Cagliari. Cagliari, p. 171 762
(unpublished thesis).

763 Over, D.J., Hauf, E., Wallace, J., Chiarello, J., Over, J.-S., Gilleaudeau, G.J., Song, Y.,
Algeo,

764 T.J., 2019. Conodont biostratigraphy and magnetic susceptibility of Upper Devonian 765 Chattanooga Shale, eastern United States: Evidence for episodic deposition and 766 disconformities. Palaeogeogr. Palaeoclimatol. Palaeoecol. 524, 137-149. 767 https://doi.org/10.1016/j.palaeo.2019.03.017.

768 Percival, L.M.E., Selby, D., Bond, D.P.G., Rakociński, M., Racki, G., Marynowski, L.,
769 Adatte, T., Spangenberg, J.E., Föllmi, K.B., 2019. Pulses of enhanced continental 770 weathering associated with multiple Late Devonian climate perturbations: Evidence from
771 osmium-isotope compositions. Palaeogeogr. Palaeoclimatol. Palaeoecol. 524, 240-249.

772 Riquier, L., Averbuch, O., Devleeschouwer, X., Tribovillard, N., 2010. Diagenetic versus
773 detrital origin of the magnetic susceptibility variations in some carbonate Frasnian774 Famennian boundary sections from Northern Africa and Western Europe: implications for
775 paleoenvironmental reconstructions. Int. J. Earth Sci. 99, 57-73.

776 Sandberg, C.A., 1976. Conodont biofacies of late Devonian *Polygnathus styriacus* Zone in
777 western United States, In: Barnes, C.R. (Ed.), Conodont Paleoecology. Geol. Assoc. 778 Canada spec. Pap. Montreal, pp. 171-186.

779 Sandberg, C.A., Morrow, J.R., Ziegler, W., 2002. Late Devonian sea-level changes, 780 catastrophic events, and mass extinctions. Geol. Soc. Am. Spec. Pap. 356, 473-487.

781 Schülke, I., 1995. Evolutive Prozesse bei *Palmatolepis* in der frühen Famenne-Stufe
782 (Conodonta, Ober-Devon). Göttinger Arbeiten zur Geologie und Pälaontologie, Göttingen. 783 Schülke, I., 1999. Conodont multielement reconstructions from the the early Famennian (Late 784 Devonian) of the Montagne Noire (southern France). Geol. Palaeontol. 31, 1-123.

785 Schülke, I., Popp, A., 2005. Microfacies development, sea-level change, and conodont 786 stratigraphy of Famennian mid- to deep platform deposits of the Beringhauser Tunnel 787 section (Rheinisches Schiefergebirge, Germany). Facies 50, 647-664.

788 Seddon, G., Sweet, W.C., 1971. An ecologic model for conodonts. J. Paleontol. 45, 869-880.

789 Spalletta, C., Perri, M.C., Over, D.J., Corradini, C. 2017. Famennian (Upper Devonian) 790 conodont zonation: revised global standard. Bull. Geosci. 92 (1), 31-57.

791 Tucker, E., 1974. Sedimentology of Palaeozoic pelagic limestones: the Devonian Griotte
792 (Southern France) and Cephalopodenkalk (Germany). Spec. Pub., Intern. Assoc.
793 Sedimentologists 1, 71-92.

794 Wendt, J., Aigner, T., 1985. Facies patterns and depositional environments of Palaeozoic
795 cephalopod limestones. Sediment. Geol. 44, 263-300. http://doi.org/10.1144/SP414.15

796 Wiederer, U., Königshof, P., Feist, R., Franke, W. and Doublier M. P. 2002. Low-grade
797 metamorphism in the Montagne Noire (S-France): Conodont Alteration Index (CAI) in 798 Palaeozoic carbonates and implications fort he exhumation of a hot metamorphic core 799 complex. Schweiz. mineral. petrogr. Mitt. 82, 393-407.

800 Ziegler, W., 1962. Taxionomy und Phylogenie oberdevonischer Conodonten und ihre 801 stratigraphische Bedeutung. Abh. hess. Landesamt. Bodenforsch. Wiesbaden.

802

803

804 **Figure captions**

805 **Figure 1**. **a)** Early Famennian (-370.3 Ma) paleogeographic map (after Franke et al., 2017 and
806 Golonka, 2020) showing the locations of the studied sections.
807 Abbreviations: SES: Sessacker (Rhenish Slate Mountains, Germany), BHT: Beringhauser
Tunnel (Rhenish Slate Mountains, Germany), PZW: Pizzul West (Carnic Alps, Italy), CT:
809 Col des Tribes (Montagne Noire, France), CM: Corona Mizziu (Sardinia, Italy), BU:
810 Buschteich (Thuringia, Germany), ERF: Erfoud (Tafilalt, SE Morocco), DGHS (DuPont GHS
811 Core, Eastern United States, after Over et al. 2019). **b)** Biostratigraphic correlation of the
the 812 studied sections.

813

814 **Figure 2**. Magnetic susceptibility curves through the Famennian (Late Devonian) for sections
815 of S-Laurussia and N-Gondwana. Ages based on Girard et al. (2020), and updated after
816 Becker et al. (2020). The curves represent the average of the MS values obtained with 2 to 5
817 measurements with the standard error in grey. Vertical dotted line: average MS values for
818 lithified marine deposits estimated to 5. 5 x 10^{-8} m3/kg (Ellwood et al. 2011a). Data of DGHS
819 (Eastern United States) are after Over et al. (2019) and data of uppermost Frasnian to lower
Famennian in Coumiac (CUQ*) and Berinhauser Tunnel (BHT*) after Riquier et al. (2010).
821 Conodont Zones after Spalletta et al. (2017).

822

823 **Figure 3**. **a)** Magnetic susceptibility curves through the Famennien (Late Devonian) at Col
824 des Tribes (CT, France) in green, Buschteich (BU, Germany) in red and Corona Mizziu (CMI
825 and CM II, Italia) in orange, Sessacker (SES) in black. **b)** Conodont biofacies through time
826 depicted as variations along the first axis of the PCA on conodont genera percentages of CT
827 (in green), BU (in red), CM (dotted line in orange), and (SES) in black. **c)** Simplified
828 transgressive-regressive cycles after Johnson et al. (1985, 1996). Conodont Zones after

Spalletta et al. (2017). Ages based on Girard et al. (2020), modified after Becker et al. (2020).

Supplementary Figure 1. Low field magnetic susceptibility (χLF) and geochemical data (Al_2O_3, SiO_2, Fe_2O_3, TiO_2, K_2O) for the PZW, CM II and CM I sections.

Supplementary Figure 2. Scatterplots reporting the MS versus selected geochemical indexes for samples from the Buschteich section (Level BU03 not figured). **a)** The zirconium (Zr) concentration (ppm); **b)** the iron (Fe) concentration (%); **c)** Fe_{exc} (%), **d)** Fe_{det} (%). The number of samples, the correlation coefficient r, and the p are reported for each diagram. Open red circles: levels after the "Enkeberg event", Red coloured circles: levels before the "Enkeberg event".

Supplementary Table 1. Magnetic susceptibility (MS) for the Col des Tribes (CT) section. MS in m^3/kg. Depth in cm. Conodont Zones after Spalletta et al. (2017). Ages based on Girard et al. (2020), and modified after Becker et al. (2020).

Supplementary Table 2. Magnetic susceptibility (MS) for the Buschteich (BU) section. MS in m^3/kg. Depth in cm. Conodont Zones after Spalletta et al. (2017). Ages based on Girard et al. (2020), and modified after Becker et al. (2020). Concentrations in Fe, Al, Zr (in ppm), and associated errors.

Supplementary Table 3. Magnetic susceptibility (MS) for the Sessacker (SES) section. MS in m^3/kg. Depth in cm. Conodont Zones after Spalletta et al. (2017). Ages based on Girard et al. (2020), and modified after Becker et al. (2020).

Supplementary Table 4. Magnetic susceptibility (MS) for the Beringhauser Tunnel (BHT) section. MS in m^3/kg. Depth in cm. Conodont Zones after Spalletta et al. (2017). Ages based on Girard et al. (2020), and modified after Becker et al. (2020).

[Tapez ici]

Supplementary Table 5. Magnetic susceptibility (MS) for the Erfoud (ERF) section. MS in m^3/kg. Depth in cm. Conodont Zones after Spalletta et al. (2017). Ages based on Girard et al. (2020), and modified after Becker et al. (2020).

Supplementary Table 6. Magnetic susceptibility (MS) for the Pizzul West (PZW) section. MS in m^3/kg. Depth in cm. Conodont Zones after Spalletta et al. (2017). Ages based on Girard et al. (2020), and modified after Becker et al. (2020).

Supplementary Table 7. Magnetic susceptibility (MS) for the Corona Mizziu II (CM II) section. MS in m^3/kg. Depth in cm. Conodont Zones after Spalletta et al. (2017). Ages based on Girard et al. (2020), and modified after Becker et al. (2020).

Supplementary Table 8. Magnetic susceptibility (MS) and low field magnetic susceptibility (χLF), ferromagnetic contribution (χFerro), hysteresis parameters (high field magnetic susceptibility (χHF)), saturation magnetization (MS), coercitive force (Hc), coercivity of remanence (Hcr), highfield remanence and viscosity decay; geochemical data for Corona Mizziu I (CM I) section.

Supplementary Table 9. Low field magnetic susceptibility (χLF), ferromagnetic contribution (χFerro), hysteresis parameters (high field magnetic susceptibility (χHF)), saturation magnetization (MS), coercitive force (Hc), coercivity of remanence (Hcr), highfield remanence and viscosity decay, geochemical data for the Corona Mizziu II (CM II) section.

Supplementary Table 10. Low field magnetic susceptibility (χLF), ferromagnetic contribution (χFerro), hysteresis parameters (high field magnetic susceptibility (χHF)), saturation magnetization (MS), coercitive force (Hc), coercivity of remanence (Hcr), highfield remanence and viscosity decay and geochemical data for the Pizzul West (PZW) section.

Supplementary Table 11. Mean MS (m^3/kg), and conodont genera percentages (pc). Names of the samples: CT (Col des Tribes), BU (Buschteich), SES (Sessacker), CM (Corona Mizziu). Ages are given by the conodont zones after Spalletta et al. (2017) and by the age model (in My). Proportions of the different genera: pcPa: *Palmatolepis*; pcPo: *Polygnathus*;

[Tapez ici]

pcAn: *Ancyrognathus* and *Ancyrodella*; pcIc: *Icriodus*; pcBi: *Bispathodus*, *Branmehla* and *Mehlina*; pcSc. *Scaphignathus* and *Alternognathus*, pcSi: *Siphonodella*.

Table 1. Correlations between MS (χLF), and ferromagnetic contribution (χFerro), high field magnetic susceptibility (χHF), coercivity of remanence (Hcr), and geochemical data using linear regression. Number of samples (N), coefficient of correlation (r) and probability (p) are given. Significant correlations marked in bold ($p < 0.05$).

		CM I			CM II			PZW		
		N	r	p	N	r	p	N	r	p
Xlf	Xferro	32	**0.69**	**0.000**	14	**0.85**	**0.000**	20	**0.87**	**0.000**
	Xhf	32	**0.82**	**0.000**	14	**0.82**	**0.000**	21	0.03	0.454
	Hcr	32	**0.68**	**0.000**	14	0.74	**0.002**	21	0.03	0.422
Xlf	Al2O3	13	0.68	**0.010**	11	0.25	0.463	17	0.005	0.785
Xhf		13	0.48	0.095	11	0.27	0.915	17	**0.84**	**0.000**
Xlf	SiO2	13	0.51	0.072	11	0.47	0.146	17	0.12	0.653
Xhf		13	0.55	0.050	11	0.49	0.122	17	**0.81**	**0.000**
Xlf	Fe2O3	13	0.70	**0.008**	11	0.67	**0.023**	17	0.13	0.613
Xhf		13	0.50	0.081	11	0.39	0.239	17	**0.92**	**0.000**
Xlf	TiO2	13	0.70	**0.008**	11	0.30	0.361	17	0.12	0.655
Xhf		13	0.48	0.096	11	0.31	0.350	17	**0.85**	**0.000**
Xlf	K2O	13	0.70	**0.008**	11	0.08	0.805	17	0.04	0.890
Xhf		13	0.45	0.123	11	0.46	0.158	17	**0.83**	**0.000**

Highlights

Early Famennian MS values differ on N-Gondwana and on S-Laurussia margins

Famennian MS values correlate with conodont biofacies

MS is a powerful tool for geodynamics

Credit Author Statement

CG Conceptualization, Fieldwork, Supervision, Funding acquisition, Writing - Original Draft

Preparation; **RF** Interpretations, Discussions, Writing**; AM** Data acquisition, geochemical and MS analyses**; JJC** Interpretations, Discussions, Writing**; ALC** Fieldwork, Sample Preparation**; PC** Interpretations, Discussions, Writing**; CC** Fieldwork, Conceptualization & Supervision

Declaration of competing interest

The authors declare that they have no known competing financial interests or personal relationships that could have appeared to influence the work reported in this paper.

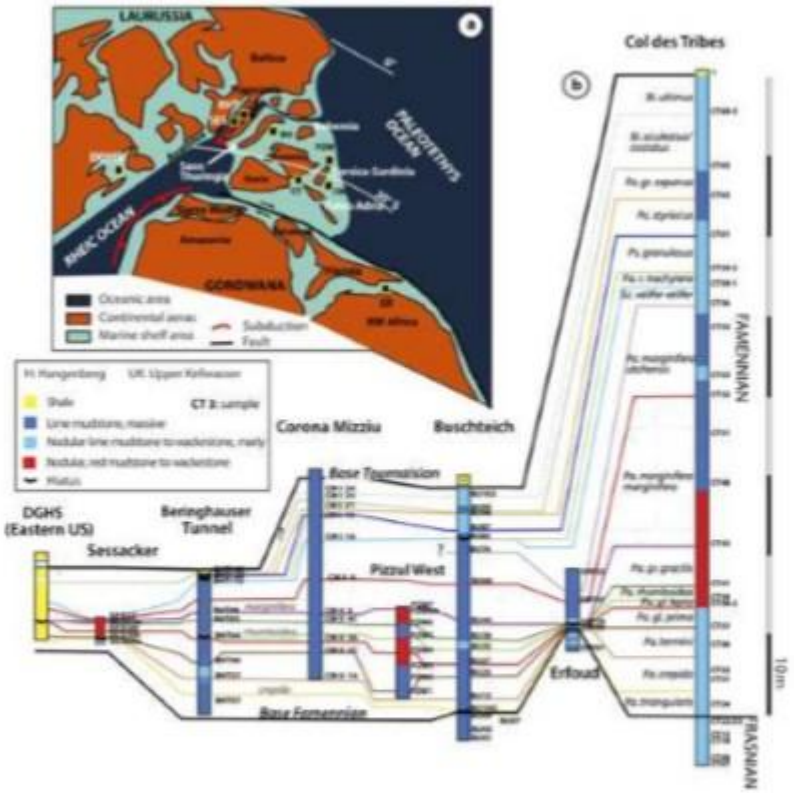

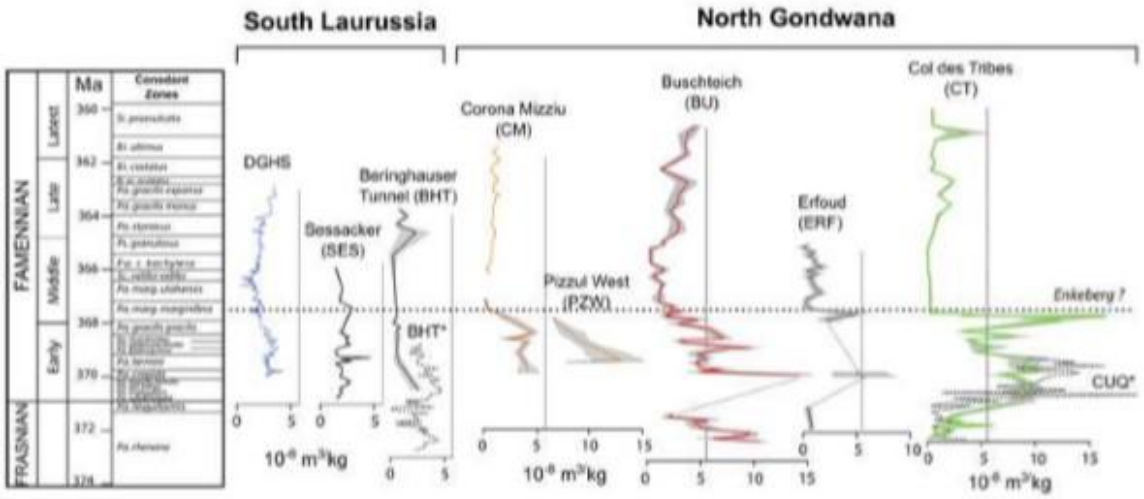

920
921

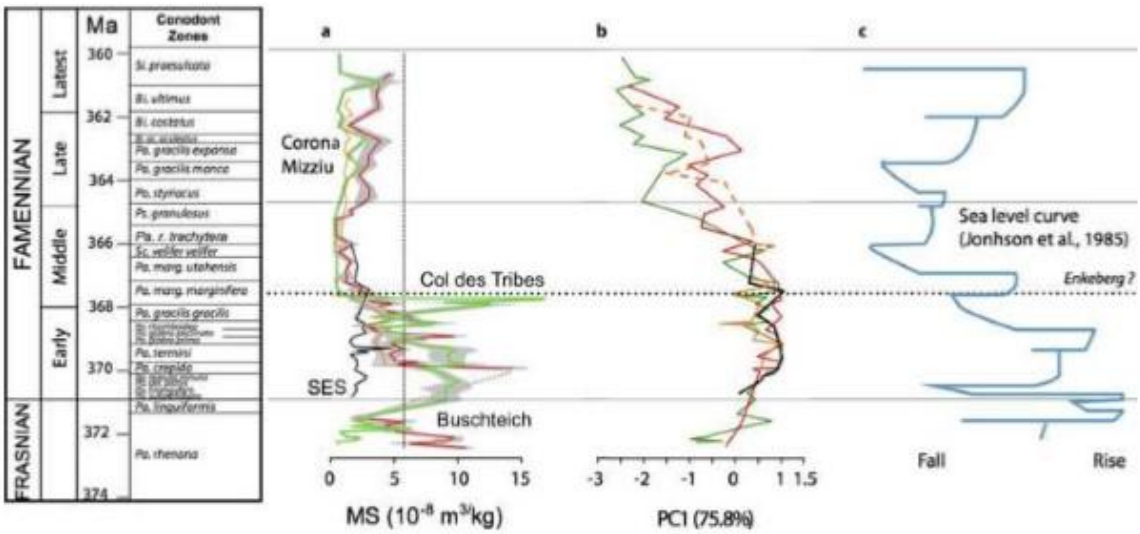

922
923 Graphical abstract

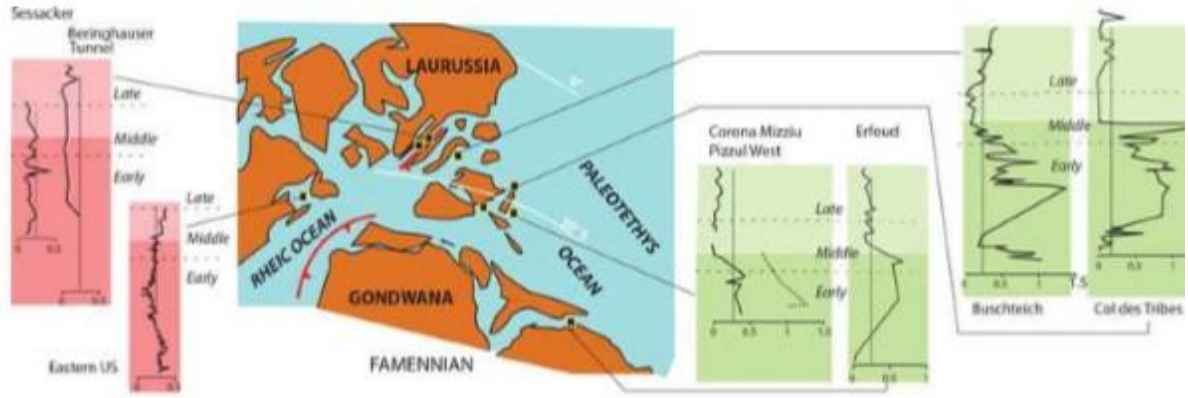
Sessacker
Beringhausen Tunnel
Late
Middle
Early
Eastern US
LAURUSSIA
RHEIC OCEAN
GONDWANA
PALEOTETHYS
OCEAN
FAMENNIAN
Corona Mizziu
Piazul West
Erfoud
Buschteich
Col des Tribes
TS

924